



Corrosion resistance of cerium-doped zinc calcium phosphate chemical conversion coatings on AZ31 magnesium alloy

Rong-chang ZENG^{1,2}, Yan HU^{1,2}, Fen ZHANG^{1,2}, Yuan-ding HUANG⁴, Zhen-lin WANG³, Shuo-qi LI^{1,2}, En-hou HAN⁵

1. College of Materials Science and Engineering, Shandong University of Science and Technology, Qingdao 266590, China;

2. State Key Laboratory of Mining Disaster Prevention and Control Co-founded by Shandong Province and the Ministry of Science and Technology, Shandong University of Science and Technology, Qingdao 266590, China;

3. School of Materials Science and Engineering, Chongqing University of Technology, Chongqing 400054, China;

4. MagIC–Magnesium Innovation Center, Helmholtz-Zentrum Geesthacht, Zentrum für Material-und Küstenforschung GmbH, Geesthacht D-21502, Germany;

5. National Engineering Center for Corrosion Control, Institute of Metals Research, Chinese Academy of Science, Shenyang 110016, China

Received 23 March 2015; accepted 29 September 2015

Abstract: Zinc calcium phosphate (Zn–Ca–P) coating and cerium-doped zinc calcium phosphate (Zn–Ca–Ce–P) coating were prepared on AZ31 magnesium alloy. The chemical compositions, morphologies and corrosion resistance of coatings were investigated through energy-dispersive X-ray spectroscopy (EDS), X-ray photoelectron spectroscopy (XPS), X-ray diffraction (XRD), electron probe micro-analysis (EPMA) and scanning electron microscopy (SEM) together with hydrogen volumetric and electrochemical tests. The results indicate that both coatings predominately contain crystalline hopeite ($\text{Zn}_3(\text{PO}_4)_2 \cdot 4\text{H}_2\text{O}$), $\text{Mg}_3(\text{PO}_4)_2$ and $\text{Ca}_3(\text{PO}_4)_2$, and traces of non-crystalline MgF_2 and CaF_2 . The Zn–Ca–Ce–P coating is more compact than the Zn–Ca–P coating due to the formation of CePO_4 , and displays better corrosion resistance than the Zn–Ca–P coating. Both coatings protect the AZ31 Mg substrate only during an initial immersion period. The micro-galvanic corrosion between the coatings and their substrates leads to an increase of hydrogen evolution rate (HER) with extending the immersion time. The addition of Ce promotes the homogenous distribution of Ca and formation of hopeite. The Zn–Ca–Ce–P coating has the potential for the primer coating on magnesium alloys.

Key words: AZ31 magnesium alloy; cerium; zinc calcium phosphate; chemical conversion coating; corrosion resistance

1 Introduction

Magnesium alloys have become the preferred alternative structural materials in the aerospace and automobile industries due to their low density, high specific strength and recyclability [1,2]. However, their applications are hindered, to a certain degree, because of their low corrosion resistance [3,4]. Thus, considerable measurements have been taken to improve the corrosion resistance of magnesium alloys. In addition to alloying [5], post processing and surface treatments including chemical conversion [6], anodic oxidation [7,8], electroplating [9], electroless plating [10], thermal

spraying [11], magnetron sputtering [12], organic coating [13], ion implantation [14], laser processing [15] and their composite coating [16] have been used. In particular, chemical conversion coatings such as the chromium [17], phosphate [17], phosphate–potassium permanganate [18], rare earth [19–21], stannate [22], silane [23,24] and phytic acid [25,26] together with fluorozirconate [27] and layered double hydroxides (LDH) [28,29] are regarded as the most effective approaches to protect magnesium alloys. Unfortunately, chromium conversion coatings are highly toxic and carcinogenic [3]. Thus, environmentally friendly conversion coatings are required.

Currently, scientists are interested in rare earth and

Foundation item: Project (51571134) supported by the National Natural Science Foundation of China; Project (2014TDJH104) supported by the SDUST Research Fund, the Joint Innovative Centre for Safe and Effective Mining Technology and Equipment of Coal Resources, Shandong Province, China; Project (cstc2012jjA50034) supported by the Natural Science Foundation of Chongqing, China

Corresponding author: Rong-chang ZENG; Tel: +86-532-80681226; E-mail: rczeng@foxmail.com

DOI: 10.1016/S1003-6326(16)64102-X

phosphate conversion coatings due to their environmentally friendly characteristics. The rare earth conversion coatings, formed by adding rare earth salts such as cerium, nitrate and lanthanum nitrate into chemical conversion baths, lead to a remarkable increase of corrosion resistance of magnesium alloys [3,30–32]. Moreover, the rare earth conversion film is utilized as the precursor for micro-arc oxidation (MAO) to obtain a cerium-containing coating. Additionally, it is found that the pre-treatment of AZ91D alloy can effectively incorporate cerium oxides into the MAO coating and improve the performance of MAO coating [33].

Phosphate conversion coatings are regarded as suitable alternatives to chromate conversion coatings because of their low toxicity and appropriate properties [34]. To date, there are six types of phosphate conversion coatings on magnesium alloys [35]: the Zn–P system [36–39], the Mn–P system [18,40,41], the barium phosphate (B–P) system [42], the molybdate phosphate (Mo–P) system [43], the Zn–Ca–P system [35,44] and the cerium phosphate (Ce–P) system [45]. Usually, the Zn–P coating contains two layers [37,46,47] with AlPO_4 , MgF_2 , $\text{Mg}_3(\text{PO}_4)_2$ and $\text{MgZn}_2(\text{PO}_4)_2$ [38]. The formation of Zn–P coating is affected by the microstructure (i.e., intermetallic compounds) of the substrate alloys [37]. The Mn–P coating on AZ91D alloy is prepared at 80 °C [40]. The Mo–P coating formed on AZ31 magnesium alloys consists of mixed phases of $\text{Mg}(\text{OH})_2$, MoO_2 , MoO_3 and MgF_2 [43]. Our previous studies [48,49] demonstrated that the introduction of Ca^{2+} ions into a zinc phosphate bath can promote the formation of a Zn–Ca–P coating and refine the microstructure of the coating, thus improving the corrosion resistance of AZ31 magnesium alloy. Moreover, a crystalline Zn–Ca–P coating with a more fine-grained structure provides a superior corrosion resistance than the Zn–P coating on the AZ31 magnesium alloy. The formation and corrosion resistance of Zn–Ca–P coating are significantly influenced by its microstructure and the chemical composition of Mg–Al alloy [50]. A further exploration revealed that the optimum temperature of a phosphating bath is 55 °C for the Zn–Ca–P coating on a Mg–Li–Ca alloy [51]. However, the microstructure of Zn–Ca–P coating on magnesium alloys still needs further improvement. Additionally, its corrosion mechanism is not yet well understood.

The present work aims to modify the microstructure and improve the corrosion resisting property of Zn–Ca–P conversion coating by doping with cerium and gain insight into the formation and corrosion mechanism of Zn–Ca–Ce–P coated alloy.

2 Experimental

2.1 Preparation of coatings

The experimental material was commercial rolled AZ31 alloy (chemical composition: 3% Al, 1% Zn and balance Mg, mass fraction), which was supplied by Beijing Guangling Jinghua Science & Technology, Co., Ltd.. The samples with dimensions of 20 mm × 20 mm × 3 mm were ground with SiC emery paper up to 2000 grit to achieve smooth surfaces. Prior to the preparation of coating, the samples were degreased in an alkaline solution, then in an acidic solution, and finally rinsed in distilled water and dried by warm air. The deposition of Zn–Ca–P coating was carried out by immersing the sample in a phosphating bath, which contained 10.0 g/L Na_2HPO_4 , 4.0 g/L NaNO_2 , 6.0 g/L $\text{Zn}(\text{NO}_3)_2$, 2.0 g/L $\text{Ca}(\text{NO}_3)_2$ and 2.0 g/L NaF. For the preparation of Zn–Ca–Ce–P coating, 1.0 g/L $\text{Ce}(\text{NO}_3)_3$ was added to the solution mentioned above. The bath pH value was adjusted to 2.5 by adding phosphoric acid. All samples were immersed in the phosphating bath at 50 °C for 20 min.

2.2 Hydrogen evolution tests

The corrosion rate of the substrate and its coatings can be monitored by the hydrogen evolution volume. The evolved hydrogen volume was read per hour during an immersion period of 24 h in 3.5% NaCl (mass fraction) solution at room temperature. The hydrogen evolution rate (HER) (R_H) can be calculated as follows:

$$R_H = V_H / st \quad (1)$$

where V_H is the hydrogen evolution volume (mL), s is the exposed area (cm^2) and t is the immersion time (h).

2.3 Surface analysis

The morphologies of the coatings before and after corrosion testing were observed using a scanning electron microscope (SEM, KYKY-2800B) equipped with an energy-dispersive X-ray spectroscope (EDS). The cross-sectional microstructures were inspected by an electron probe micro-analyser (EPMA, JXA-8230). The compositions of the coatings were identified by X-ray diffraction (XRD, D/Max 2500PC) and X-ray photoelectron spectroscopy (XPS).

3 Results

3.1 Surface morphologies

The surface morphologies of Zn–Ca–Ce–P and Zn–Ca–P coatings are shown in Fig. 1. The Zn–Ca–Ce–P coating has a long, ridge-like crystalline

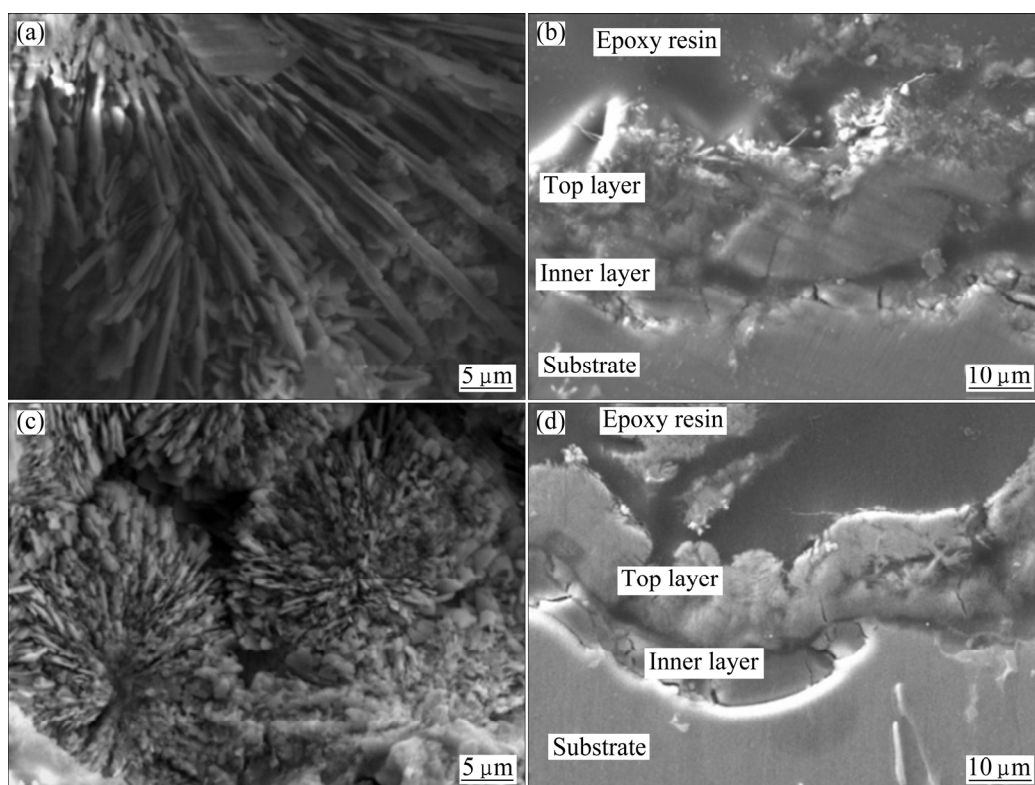


Fig. 1 SEM images (a, c) and cross-sectional views (b, d) of Zn–Ca–Ce–P coating (a, b) and Zn–Ca–P coating (c, d)

structure (1–2 μm in thickness) and short, flake-shaped crystalline precipitates with particles embedded between the ridges (Fig. 1(a)). The cross-sectional view of Zn–Ca–Ce–P coating (Fig. 1(b)) reveals that it contains a double-layer structure, an outer layer with a ridge-like crystalline microstructure and an inner layer with a compact microstructure with micro-cracks. However, no through cracks are found on the whole Zn–Ca–Ce–P coating (Fig. 1(b)). It is worth noting that the Zn–Ca–P coating resembles a flower-like morphology with refined microstructure and cracks, which are obviously observed among the flower-like structures (Fig. 1(c)). This result is in agreement with the previous study [50]. However, the Zn–Ca–P coating has considerable through cracks (Fig. 1(d)), which leads to a reduction in the compactness of Zn–Ca–P coating and its adhesion to the substrate.

3.2 Chemical compositions and constitutions

Figure 2 shows the SEM images and EDS patterns of coatings. Both coatings are composed of elements O, Zn, P, Mg, F, Al and Ca (Table 1). The existence of C is ascribed to the sprayed carbon on the surface of samples prior to the EPMA examination. The Zn–Ca–Ce–P coating exhibits a higher Mg content. The high content of F in the non-crystalline areas (points *A* and *C* in Fig. 2(a) and point *C* in Fig. 2(b)) implies the possible presence of MgF_2 , CeF_3 and CaF_2 , whereas no F is detected in the crystallized areas (point *B* in Fig. 2(a) and

points *A* and *B* in Fig. 2(b)). This scenario demonstrates that MgF_2 , CeF_3 and CaF_2 are heterogeneously distributed in these two coatings. The presence of Zn and Ca is derived from $\text{Zn}(\text{NO}_3)_2$ and $\text{Ca}(\text{NO}_3)_2$, respectively, in solutions. Our previous investigation [49] also indicated that CaHPO_4 and $\text{Ca}_3(\text{PO}_4)_2$ were located in the outer layer of Zn–Ca–P coating. The contents of Zn and P in Zn–Ca–Ce–P coating are higher than those in Zn–Ca–P coating (Table 1). Higher content of Zn, in comparison with that in the Zn–Ca–P coating, may be attributed to higher crystallinity of the Zn–Ca–Ce–P coating. This result suggests that a high amount of hopeite covers the Zn–Ca–Ce–P coating.

The elemental mappings from the cross-sectional perspective (Fig. 3) show that the contents of Mg and P in the interior layer are significantly higher than those in the exterior layer for both coatings. It can be concluded that $\text{Mg}_3(\text{PO}_4)_2$ is located in the inner layer of two coatings. This result is consistent with our previous investigation [49]. It is worth noting that the content of Zn in the exterior layer of coatings is considerably higher than that in the interior layer, indicating that a high amount of hopeite deposits on the surface. The distribution of Ca is more homogeneous in the Zn–Ca–Ce–P coating than that in the Zn–Ca–P coating (Fig. 3). The element Ce is not detected by EDS due to its lower content. This novel finding demonstrates that the introduction of Ce^{3+} ions promotes the homogeneity

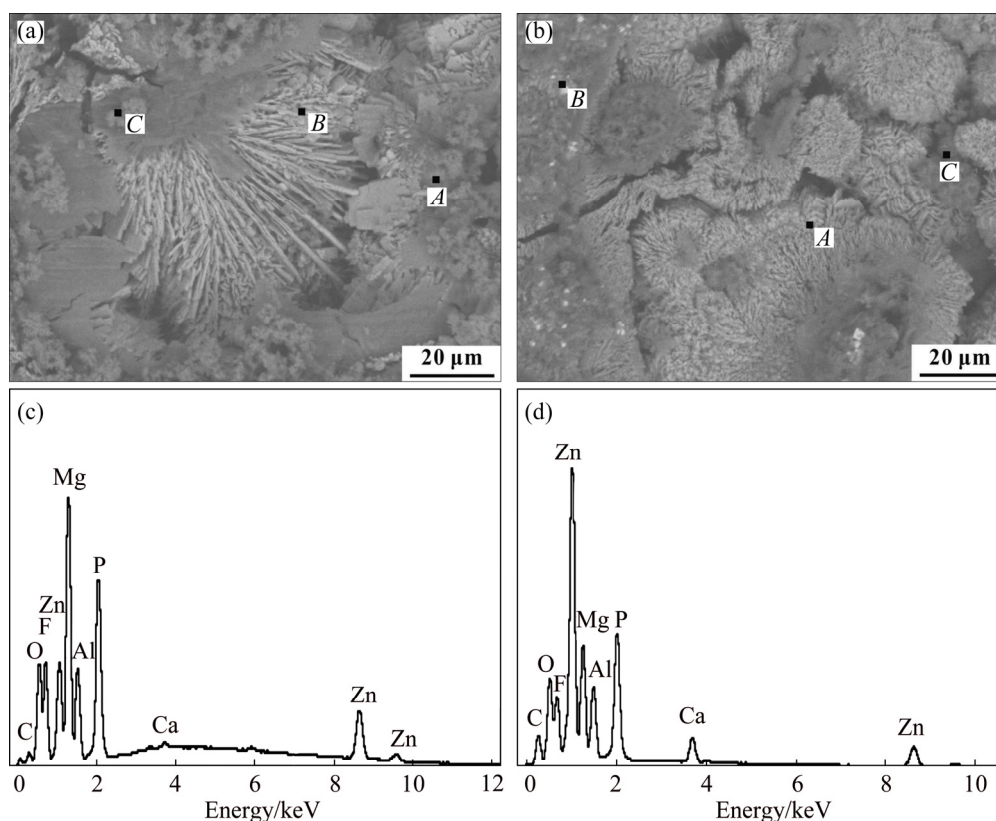


Fig. 2 SEM images (a, b) and corresponding EDS mappings of point C (c) and point B (d) of Zn–Ca–Ce–P (a, c) and Zn–Ca–P (b, d) coatings

Table 1 Chemical compositions of coatings in different positions (mass fraction, %)

Coating	Point	Element							
		C	O	Mg	F	Al	P	Zn	Ca
Zn–Ca– Ce–P	A	6.40	39.12	9.59	4.75	3.75	13.59	22.39	0.41
	B	10.61	31.66	7.03	0	1.66	18.42	30.41	0.21
	C	9.33	17.21	17.14	19.73	5.80	10.66	19.72	0.41
Zn–Ca–P	A	25.36	36.83	6.18	0	0.59	16.02	14.76	0.26
	B	5.14	54.80	6.20	0	7.63	13.71	12.04	0.48
	C	21.87	22.52	8.67	20.16	5.03	8.87	10.65	2.23

of Ca distribution. Further investigations by XRD confirm this finding.

The XRD patterns of both coatings are quite different from each other (Fig. 4). The peaks of α -Mg phase designate the microstructure of AZ31 Mg alloy substrate. The diffraction peaks of tetra-hydrated zinc phosphate ($\text{Zn}_3(\text{PO}_4)_2 \cdot 4\text{H}_2\text{O}$) manifest a higher intensity in the Zn–Ca–Ce–P coating than that in the Zn–Ca–P coating. The weak diffraction peaks of $\text{Mg}_3(\text{PO}_4)_2$, CePO_4 and $\text{Ca}_3(\text{PO}_4)_2$ are detected in the Zn–Ca–Ce–P coating, which proves the existence of traces of $\text{Mg}_3(\text{PO}_4)_2$, CePO_4 and $\text{Ca}_3(\text{PO}_4)_2$ that become the nuclei of the coating. The peak of ZnO is found in the Zn–Ca–P coating [52]. The ZnO originates from the dehydration of $\text{Zn}(\text{OH})_2$. MgF_2 , CeF_3 and CaF_2 are not identified by

XRD due to their noncrystalline structures.

The compositions of two coatings were probed by XPS to prove the existence of cerium salts. The XPS patterns of two coatings are shown in Fig. 5. Figure 5(a) shows that the Zn–Ca–Ce–P coating mainly consists of Mg, Zn, P, O, F, Ca and Ce, while Fig. 5(b) indicates that the Zn–Ca–P coating includes Mg, Zn, P, O, F and Ca. Meanwhile, the presence of C may be due to adventitious hydrocarbons from the environment.

Figure 6 shows the high-resolution XPS patterns of Zn, P, Ce and O elements in the Zn–Ca–Ce–P coating. The high-resolution spectrum of Zn 2p (Fig. 6(a)) is divided into two peaks, which correspond to $\text{Zn}_3(\text{PO}_4)_2 \cdot 4\text{H}_2\text{O}$ and ZnO [49]. The P 2p peak corresponds to CePO_4 , $\text{Zn}_3(\text{PO}_4)_2 \cdot 4\text{H}_2\text{O}$, $\text{Ca}_3(\text{PO}_4)_2$ and

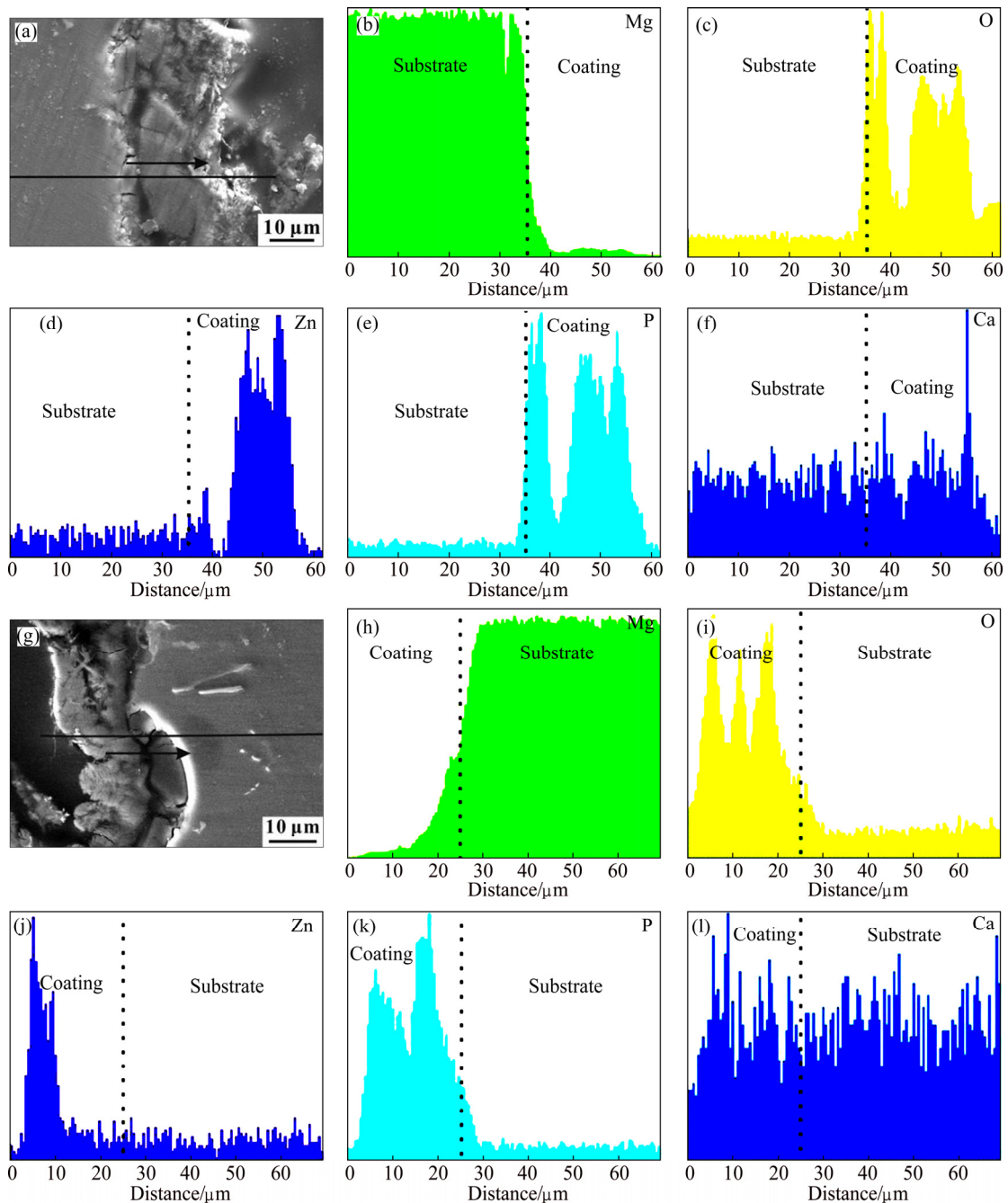


Fig. 3 SEM images (a, g) and linear scanning mappings (b–f, h–l) of cross-sectional perspective of Zn–Ca–Ce–P coating (a–f) and Zn–Ca–P coating (g–l)

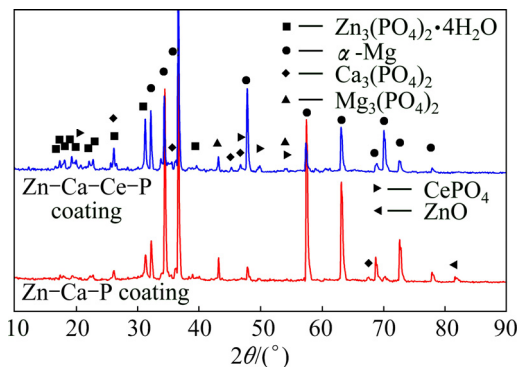


Fig. 4 XRD patterns of both coatings formed on AZ31 Mg alloy

CaHPO₄ (Fig. 6(b)). The Ce 3d peaks reveal the presence of CePO₄ (Fig. 6(c)). The high-resolution spectrum of O 1s also confirms this result (Fig. 6(d)).

The high-resolution XPS patterns of Zn, P, Ca and O in the Zn–Ca–P coating are shown in Fig. 7. Apparently, the spectrum of Zn 2p shown in Fig. 7(a) is consistent with that shown in Fig. 6(a), proving the existence of Zn₃(PO₄)₂·4H₂O and ZnO. The P 2p peak corresponds to Zn₃(PO₄)₂·4H₂O, Ca₃(PO₄)₂ and CaHPO₄ (Fig. 7(b)). The high-resolution spectrum of Ca 2p can be decomposed into two peaks assigned to Ca 2p_{3/2} and Ca 2p_{1/2} peaks (Fig. 7(c)), and the Ca 2p_{1/2} peak is the satellite peak. The Ca 2p_{3/2} peak is assigned to CaF₂,

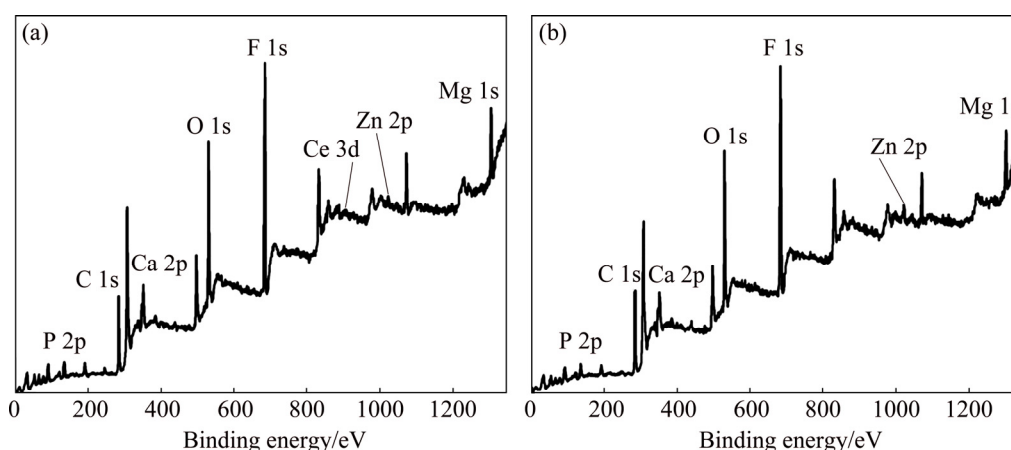


Fig. 5 XPS patterns of Zn-Ca-Ce-P coating (a) and Zn-Ca-P coating (b)

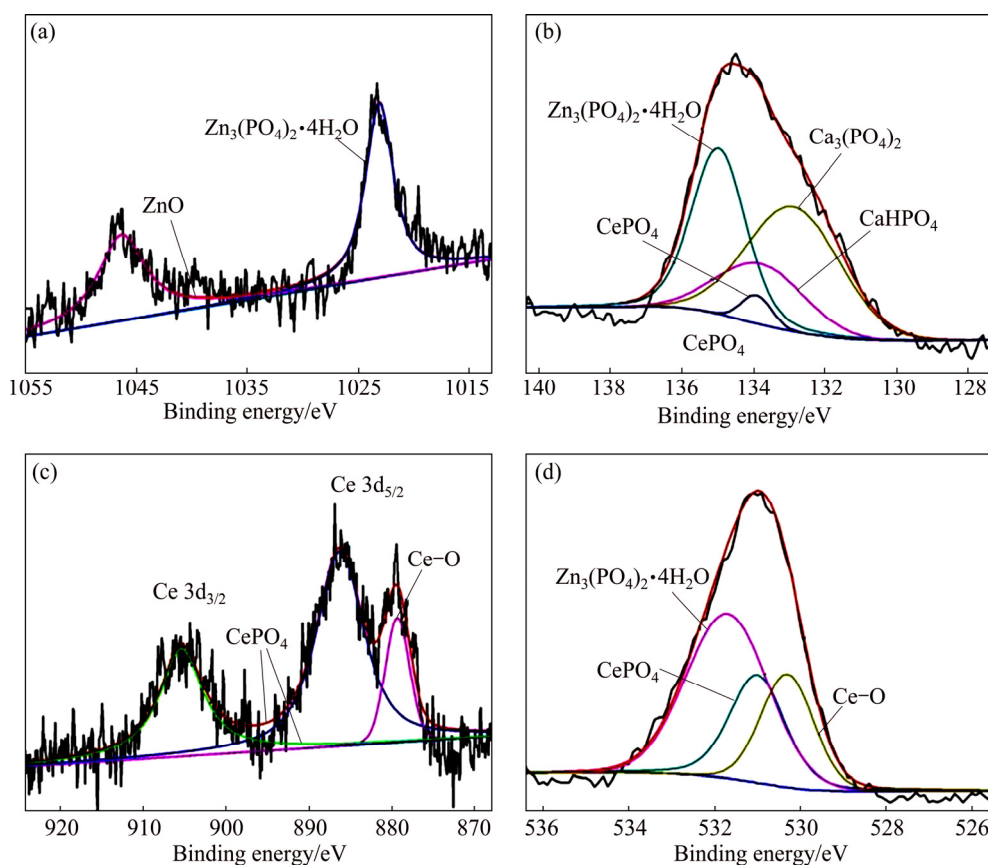


Fig. 6 High-resolution XPS patterns of Zn-Ca-Ce-P coating: (a) Zn 2p; (b) P 2p; (c) Ce 3d; (d) O 1s

$\text{Ca}_3(\text{PO}_4)_2$ and CaHPO_4 . The compositions shown in O 1s peak shown in Fig. 7(d) are in accordance with those shown in Zn, P and Ca peaks. The results not only agree with the EDS and XRD results but also further identify the presence of CePO_4 in the Zn-Ca-Ce-P coating.

4 Discussion

4.1 Formation mechanism of Zn-Ca-Ce-P coating

The formation of Zn-Ca-Ce-P coating may be

different from that of Zn-Ca-P coating that was previously studied [50] because of the introduction of $\text{Ce}(\text{NO}_3)_3$. Once the Mg alloys are immersed in an acidic phosphating bath, the α -Mg phase adjacent to the intermetallic compounds such as AlMn particles [49,50] is preferentially corroded according to the following electrochemical reactions (Fig. 8(a)):



Ce^{3+} ions are oxidized to Ce^{4+} ions in the weakly

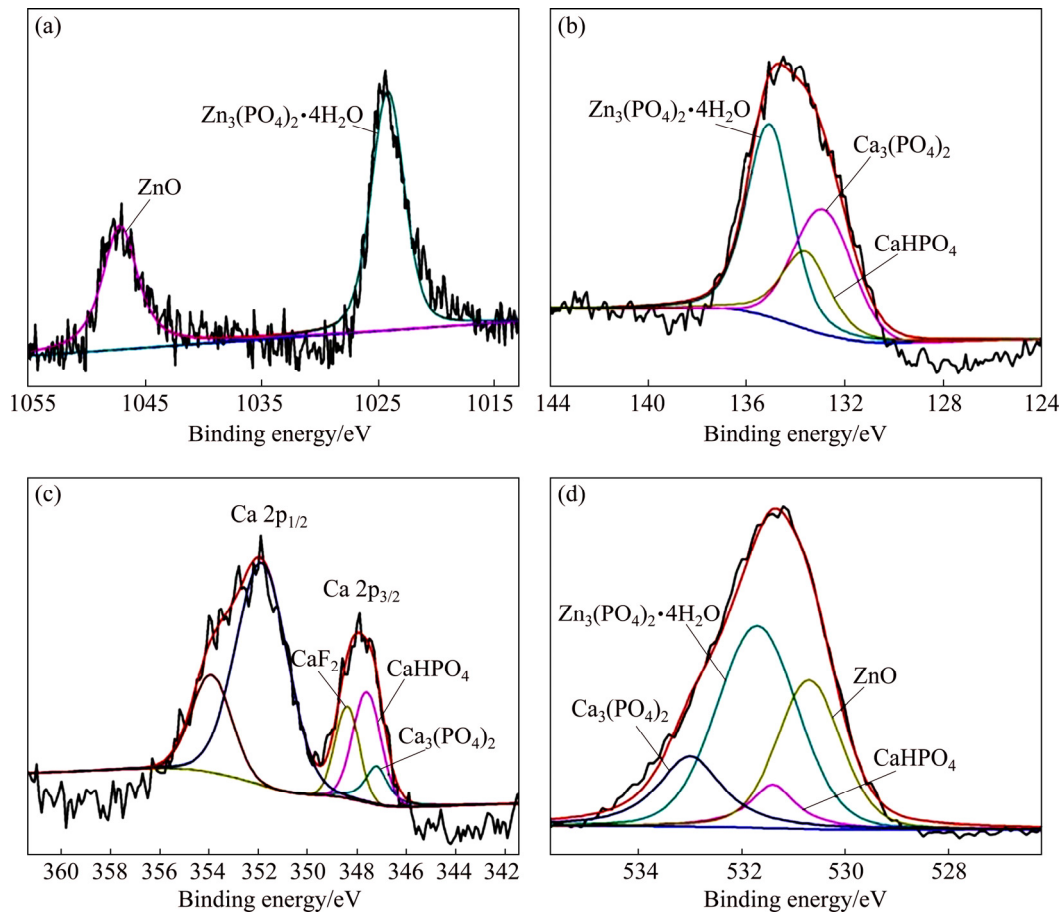
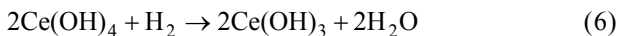
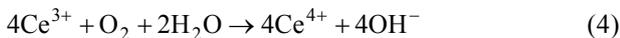


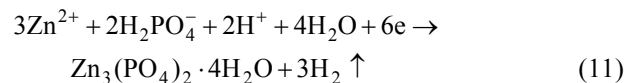
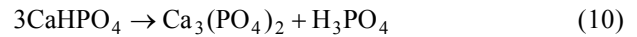
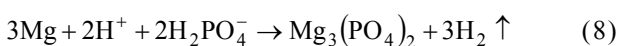
Fig. 7 High-resolution XPS patterns of Zn–Ca–P coating: (a) Zn 2p; (b) P 2p; (c) Ca 2p; (d) O 1s

acidic solution [54], leading to the formation of $\text{Ce}(\text{OH})_4$ precipitates (Reactions (4) and (5)). Therefore, a CePO_4 precipitate (Fig. 8(b)) preferentially forms because its solubility product constant (2.0×10^{-48}) is much lower than that of $\text{Ca}_3(\text{PO}_4)_2$ compound (2.0×10^{-29}). The following reactions occur successively in the acidic phosphating bath [53,54].



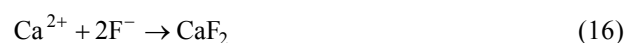
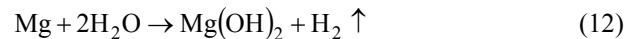
The stability of CePO_4 is higher than that of $\text{Ce}(\text{OH})_3$, especially in acid solution. The formation of CePO_4 (Fig. 6(c)) promotes the compactness of Zn–Ca–Ce–P coating by reducing the amount of water trapped in the crystal [53].

At the same time, $\text{Mg}_3(\text{PO}_4)_2$ (Fig. 8(c)), $\text{Ca}_3(\text{PO}_4)_2$ (Fig. 8(d)) and $\text{Zn}_3(\text{PO}_4)_2 \cdot 4\text{H}_2\text{O}$ (Fig. 8(e)) form on the surface of alloy [48–50]:



$\text{Zn}_3(\text{PO}_4)_2 \cdot 4\text{H}_2\text{O}$ is the main component of Zn–Ca–P coating [49]. Once the hopeite ($\text{Zn}_3(\text{PO}_4)_2 \cdot 4\text{H}_2\text{O}$) initially forms, Reaction (11) would not be interrupted until the film covers the whole surface (Fig. 8(f)).

Our previous work [52] has proved that traces of MgF_2 and MgO may form according to Reactions (13) and (14), respectively. Meanwhile, CeF_3 and CaF_2 also form according to Reactions (15) and (16), respectively.



Additionally, during the phosphating process, Zn^{2+} can obtain the electrons coming from the dissolution of magnesium and may become single zinc and deposit on

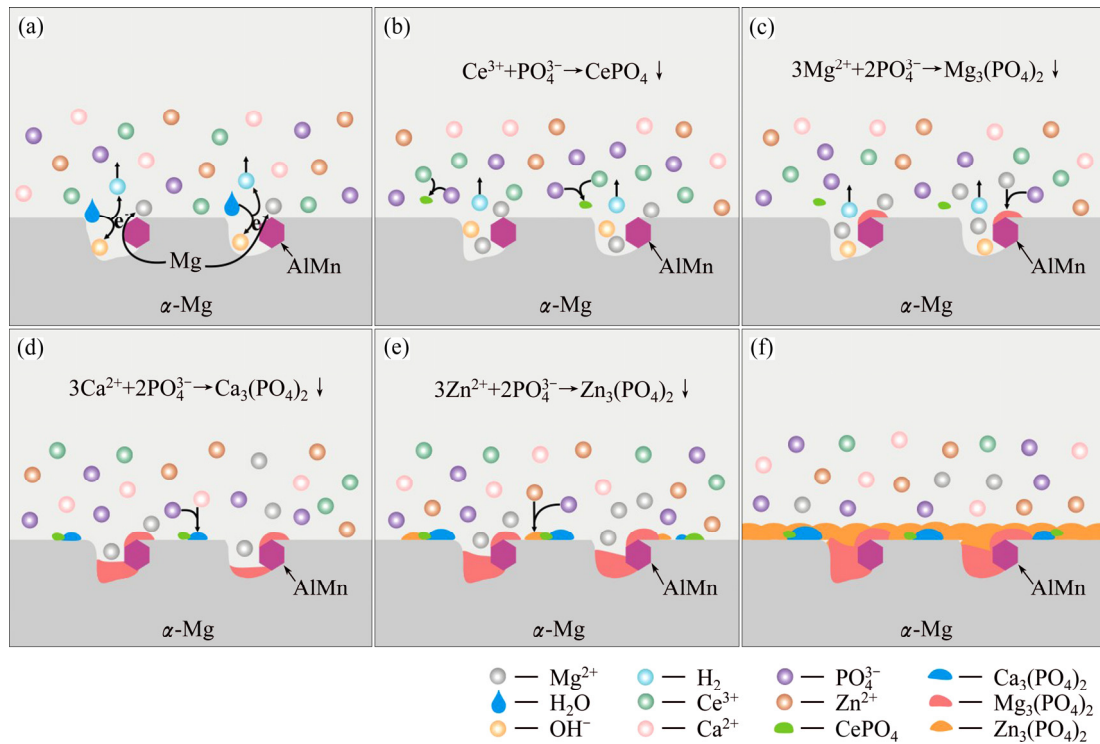
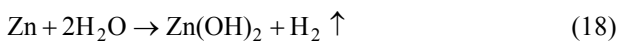


Fig. 8 Schematic diagrams of formation of Zn–Ca–Ce–P coating: (a) Dissolution of α -Mg matrix neighbouring AlMn-phase and hydrogen release; (b) Formation of nucleus of cerium phosphate; (c) Nuclei formation of magnesium phosphate; (d) Formation of calcium phosphate; (e) Formation of zinc phosphate nucleus; (f) Coalescence of zinc phosphate nuclei and formation of crystalline zinc phosphate coating

the surface [36,48,52]:



Nevertheless, Zn cannot stay in the aggressive environment for a long time. It transforms into ZnO via the following reactions [52]:



Consequently, $\text{Zn}_3(\text{PO}_4)_2 \cdot 4\text{H}_2\text{O}$ and ZnO are detected by XRD in the Zn–Ca–P coating.

According to above discussion, the formation processes of Zn–Ca–Ce–P coating follow six steps: 1) the dissolution of α -Mg matrix around the AlMn phase and the release of hydrogen (Fig. 8(a)); 2) the nuclei of cerium phosphate formed initially and uniformly in solution (Fig. 8(b)); 3) the nuclei formation of magnesium phosphate (Fig. 8(c)); 4) the formation of calcium phosphate and its precipitation on the surface of alloy with cerium phosphate, promoting the uniform formation of the dispersive nuclei of calcium phosphate (Fig. 8(d)); 5) the formation of zinc phosphate precipitates (Fig. 8(e)); 6) the coalescence of zinc phosphate precipitates mixed with calcium phosphate and cerium phosphate, and the formation of a crystalline zinc phosphate coating (Fig. 8(f)).

4.2 Corrosion mechanism of Zn–Ca–Ce–P coated alloy

Based on the corrosion resistance derived from the hydrogen evolution (Fig. 9), the HERs of both coatings continuously increase with increasing the immersion time, whereas the HER of substrate does not rise after an immersion time of 6 h and descends successively and slowly. Figure 9 shows that the corrosion processes of coatings and substrate follow three stages. At stage I, both of the coatings have a lower corrosion rate than the substrate in an immersion time of 11 h. At stage II, the Zn–Ca–P coating has the highest corrosion rate, while the Zn–Ca–Ce–P coating has the lowest value. At stage III, the corrosion rates of both coatings are higher than that of the substrate after immersion for 17 h.

At stage I, both of the coatings have a lower corrosion rate than the substrate because of the protection from the phosphate coating. A similar observation was also reported in Refs. [31,49]. The rapid increase of HER of the substrate during the initial stage is attributed to the dissolution of magnesium. However, at stages II and III, due to the formation and thickening of $\text{Mg}(\text{OH})_2$ precipitate, which inhibits the attack from Cl^- ions, the HER of substrate subsequently exhibits a slow decrease. In these stages, the HERs of Zn–Ca–Ce–P and Zn–Ca–P coatings surpass that of substrate,

which is associated with the existence of coating defects such as voids and micro-cracks (Figs. 1(b) and (d)).

Figure 10 displays the polarization curves of AZ31 Mg substrate and coated samples. The open corrosion potentials (OCP), φ_{corr} , of Zn–Ca–Ce–P and Zn–Ca–P coatings are higher and the corrosion current densities, J_{corr} , are lower than that of AZ31 alloy (Table 2). Especially, the J_{corr} of Zn–Ca–Ce–P coating decreases by almost one order of magnitude. This result is in accordance with the HER, indicating that the Zn–Ca–Ce–P and Zn–Ca–P coatings protect the alloy effectively in the initial immersion stage

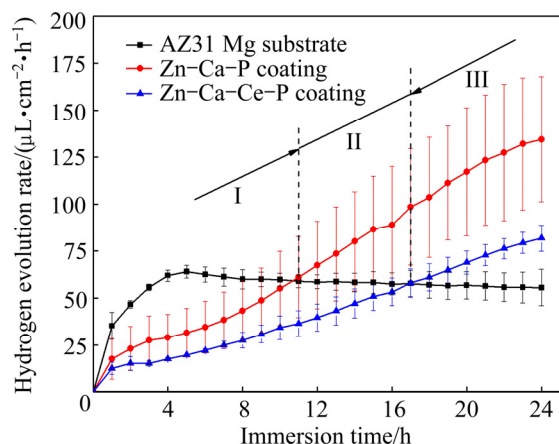


Fig. 9 Hydrogen evolution rates of AZ31 Mg substrate and its coatings in 3.5% NaCl solution

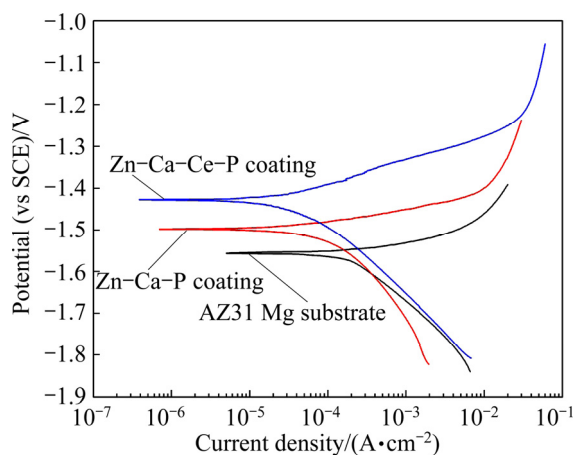


Fig. 10 Polarization curves of AZ31 Mg substrate and its coatings in 3.5% NaCl solution

Table 2 Electrochemical parameters obtained from polarisation curves in 3.5% NaCl solution

Sample	φ_{corr} (vs SCE)/V	J_{corr} (A·cm ⁻²)
AZ31 Mg alloy	-1.55	2.04×10^{-4}
Zn–Ca–P coating	-1.49	1.12×10^{-4}
Zn–Ca–Ce–P coating	-1.43	4.50×10^{-5}

The localised exfoliation or detachment of the coatings (marked by arrows in Fig. 11) occurs [46] and the substrate is exposed to the solution. The Zn–Ca–Ce–P coating has less cracks than the Zn–Ca–P coating, and the exposed areas of the substrate in the Zn–Ca–Ce–P coating are smaller (Fig. 11(a)) than those in the Zn–Ca–P coating (Fig. 11(b)). The Zn–Ca–Ce–P coating thus has a lower corrosion rate than the Zn–Ca–P coating.

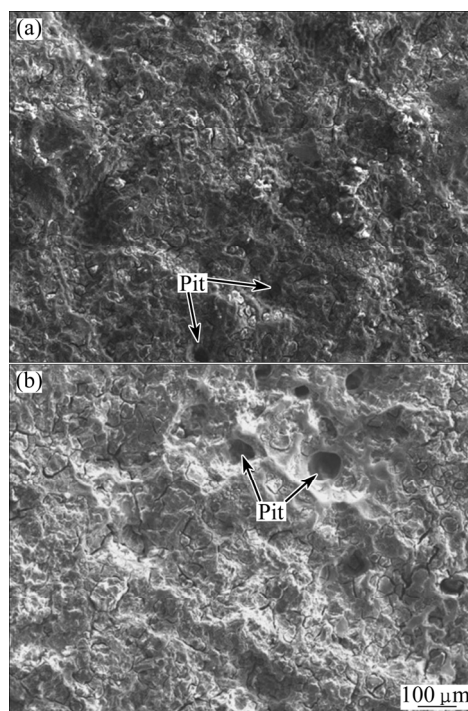


Fig. 11 SEM images of coatings after immersion for 24 h in 3.5% NaCl solution: (a) Zn–Ca–Ce–P coating; (b) Zn–Ca–P coating

The schematic diagram in Fig. 12 illustrates the corrosion mechanism of Zn–Ca–Ce–P-coated alloy. After immersing in 3.5% NaCl solution, the corrosion processes can be divided into three stages. At stage I, water rapidly diffuses into the coating, and then the defects and micro-cracks inside the coating can provide a path for the penetration of water and Cl^- ions into the substrate (Fig. 12(a)). At stage II, the secondary phase/substrate interface is exposed to the solution. The AlMn phase, having a higher corrosion potential than the α -Mg [55], acts as the micro cathode; whereas the Mg substrate acts as the micro anode. The micro-galvanic corrosion thus occurs, resulting in the formation of $\text{Mg}(\text{OH})_2$ with a prolonged period of immersion (Fig. 12(b)). At stage III, the formation of $\text{Mg}(\text{OH})_2$ seals the voids and cracks of coatings with extended immersion time. Unfortunately, the corrosion still occurs in the sealed cracks and some of the coating peels off due to the continuous generation of H_2 underneath the

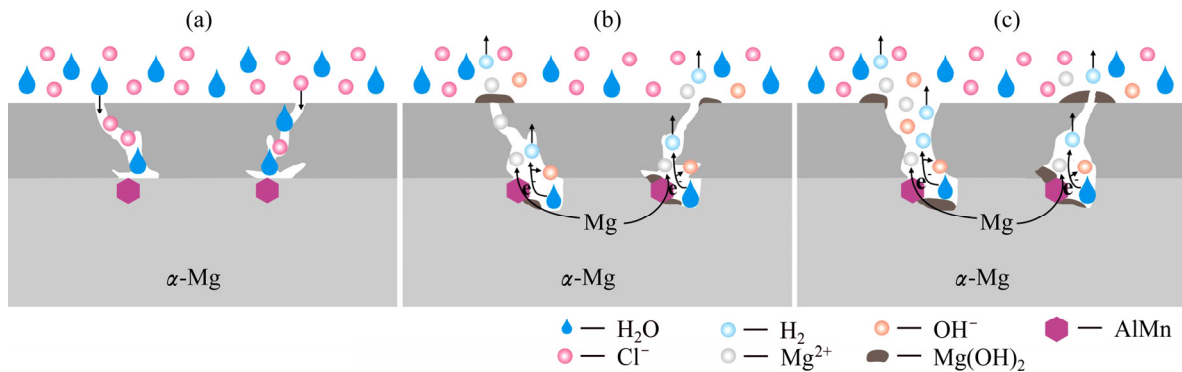


Fig. 12 Corrosion mechanism of Zn-Ca-Ce-P coated AZ31 Mg alloy: (a) Stage I; (b) Stage II; (c) Stage III

coating. More substrate is exposed to the solution which accelerates the corrosion rate (Fig. 12(c)). In the view of the HERs of the coated alloys, the corrosion initiation of the Zn-Ca-Ce-P coated alloy is significantly delayed relative to that of the Zn-Ca-P coated alloy. This consequence implies that the chemical conversion coating can hardly protect the substrate from the corrosion for a long immersion time.

5 Conclusions

1) The Zn-Ca-Ce-P coating displays a more compact double-structure with a ridge-like inner layer and a flake-like outer layer, while the Zn-Ca-P coating has a flower-like morphology with a considerable number of cracks and defects. Both coatings contain traces of noncrystalline products. The Zn-Ca-P coating predominantly consists of $Zn_3(PO_4)_2 \cdot 4H_2O$, $Mg_3(PO_4)_2$, $Ca_3(PO_4)_2$ and small amount of MgF_2 , CaF_2 and Zn/ZnO , while the Zn-Ca-Ce-P coating contains traces of $CePO_4$ and CeF_3 besides above compounds.

2) The introduction of Ce promotes the homogeneous distribution of Ca, the nuclei formation of hopeite, and the compactness of Zn-Ca-Ce-P coating, thus resulting in better corrosion resistance than the Zn-Ca-P coating. Both Zn-Ca-Ce-P and Zn-Ca-P coatings improve the corrosion resistance of AZ31 Mg substrate only over a limited immersion period.

3) The continuous decrease of corrosion resistance of coatings is attributed to the presence of micro-cracks and through-voids inside the coatings. The micro-galvanic corrosion occurs between the secondary phases and the magnesium substrate, leading to an enlargement in the exposed area of substrate, and an increase of HER over the immersion time.

References

- [1] ZENG Rong-chang, KE Wei, XU Yong-bo, HAN En-hou, ZHU Zi-yong. Recent development and application of magnesium alloys [J]. *Acta Metallurgica Sinica*, 2001, 37(7): 673–685. (in Chinese)
- [2] SONG Guang-ling. Recent progress in corrosion and protection of magnesium alloys [J]. *Advanced Engineering Materials*, 2005, 7(1): 563–586.
- [3] WANG Xi-mei, ZHU Li-qun, HE Xiang, SUN Feng-lou. Effect of cerium additive on aluminum-based chemical conversion coating on AZ91D magnesium alloy [J]. *Applied Surface Science*, 2013, 280(1): 467–473.
- [4] SONG Guang-ling. *Corrosion and protection of magnesium alloys [M]*. 2nd ed. Beijing: Chemistry Industry Press, 2006. (in Chinese)
- [5] ZENG Rong-chang, SUN Lu, ZHENG Yu-feng, CUI Hong-zhi, HAN En-hou. Corrosion and characterisation of dual phase Mg-Li-Ca alloy in Hank's solution: The influence of microstructural features [J]. *Corrosion Science*, 2014, 79: 69–82.
- [6] HAN En-hou, ZHOU Wan-qiu, SHAN Da-yong, KE Wei. Corrosion and protection of magnesium alloy AZ31D by a new conversion coating [J]. *Materials Science Forum*, 2003, 419–422: 879–882.
- [7] CHEN Jun, ZENG Rong-chang, HUANG Wei-jiu, ZHENG Zi-qing, WANG Zhen-lin, WANG Jun. Characterization and wear resistance of macro-arc oxidation coating on magnesium alloy AZ91 in simulated body fluids [J]. *Transactions of Nonferrous Metals Society of China*, 2008, 18(S1): s361–s364.
- [8] ZHANG R F, ZHANG S F. Formation of micro-arc oxidation coatings on AZ91HP magnesium alloys [J]. *Corrosion Science*, 2009, 51(12): 2820–2825.
- [9] WU Chao-yun, ZHANG Jin. Corrosion protection of Mg alloys by cathodic electrodeposition coating pretreated with silane [J]. *Journal of Coatings Technology and Research*, 2010, 7(6): 727–735.
- [10] LIU Zhen-min, GAO Wei. Electroless nickel plating on AZ91 Mg alloy substrate [J]. *Surface and Coatings Technology*, 2006, 200(16): 5087–5093.
- [11] MAJUMDAR J D, BHATTACHARYYA U, BISWAS A, MANNA I. Studies on thermal oxidation of Mg-alloy (AZ91) for improving corrosion and wear resistance [J]. *Surface and Coatings Technology*, 2008, 202(15): 3638–3642.
- [12] ZENG Rong-chang, JIANG Ke, LI Shuo-qi, ZHANG Fen, CUI Hong-zhi, HAN En-hou. Mechanical and corrosion properties of Al/Ti film on magnesium alloy AZ31B [J]. *Frontiers of Materials Science*, 2015, 9(1): 66–76.
- [13] NG W F, WONG M H, CHENG F T. Stearic acid coating on magnesium for enhancing corrosion resistance in Hanks' solution [J]. *Surface and Coatings Technology*, 2010, 204(11): 1823–1830.
- [14] LIU C L, XIN Y C, TIAN X B, CHU P K. Corrosion behavior of AZ91 magnesium alloy treated by plasma immersion ion implantation and deposition in artificial physiological fluids [J]. *Thin Solid Films*, 2007, 516(2): 422–427.
- [15] WANG Jing-feng, QIN Bin, WU Xia, PAN Fu-sheng, TANG Ai-tao. Current status and development of research on anti-corrosion

- technology for magnesium alloys [J]. *Surface Technology*, 2008, 37(5): 71–74.
- [16] ZENG Rong-chang, QI Wei-chen, SONG Ying-wei, HE Qin-kun, CUI Hong-zhi, HAN En-hou. In vitro degradation of MAO/PLA coating on Mg–1.21Li–1.12Ca–1.0Y alloy [J]. *Frontiers of Materials Science*, 2014, 8(4): 343–353.
- [17] HAMDY A S, FARAHAT M. Chrome-free zirconia-based protective coatings for magnesium alloys [J]. *Surface and Coatings Technology*, 2010, 204(6): 2834–2840.
- [18] ZHOU Wan-qiu, SHAN Da-yong, HAN En-hou, KE Wei. Structure and formation mechanism of phosphate conversion coating on die-cast AZ91D magnesium alloy [J]. *Corrosion Science*, 2008, 50(2): 329–337.
- [19] ARDELEAN H, FRATEUR I, MARCUS P. Corrosion protection of magnesium alloys by cerium, zirconium and niobium-based conversion coatings [J]. *Corrosion Science*, 2008, 50(7): 1907–1918.
- [20] ZUO Ke, WANG Xin, LIU Wei, ZHAO Yue. Preparation and characterization of Ce–silane–ZrO₂ composite coatings on 1060 aluminum [J]. *Transactions of Nonferrous Metals Society of China*, 2014, 24(5): 1474–1480.
- [21] JIANG Qiong, MIAO Qiang, TONG Fei, XU Yi, REN Bei-lei, LIU Zhi-mei, YAO Zheng-jun. Electrochemical corrosion behavior of arc sprayed Al–Zn–Si–RE coatings on mild steel in 3.5% NaCl solution [J]. *Transactions of Nonferrous Metals Society of China*, 2014, 24(8): 2713–2722.
- [22] LIN C S, LIN H C, LIN K M, LAI W C. Formation and properties of stannate conversion coatings on AZ61 magnesium alloys [J]. *Corrosion Science*, 2006, 48(1): 93–109.
- [23] ZENG Rong-chang, LIU Li-jun, PANG Ting-ting, ZHANG Fen, ZHANG Wei-wei, LI Shuo-qi, CUI Hong-zhi, HAN En-hou. Corrosion resistance of silane-modified hydroxide zinc carbonate film on AZ31 magnesium alloy [J]. *Acta Metallurgica Sinica (English Letters)*, 2015, 28(3): 373–380.
- [24] ZENG Rong-chang, CHEN Jun, KUANG Jun, ZHANG Jin, WANG Ying. Influence of silane on corrosion resistance of magnesium alloy AZ31 with thermally sprayed aluminum coatings [J]. *Rare Metals*, 2010, 29(2): 193–197.
- [25] LIU Jian-rui, GUO Yi-na, HUANG Wei-dong. Study on the corrosion resistance of phytic acid conversion coating for magnesium alloys [J]. *Surface and Coatings Technology*, 2006, 201(3): 1536–1541.
- [26] GUPTA R K, MENSAR-DARKWA K, SANKAR J, KUMAR D. Enhanced corrosion resistance of phytic acid coated magnesium by stearic acid treatment [J]. *Transactions of Nonferrous Metals Society of China*, 2013, 23(5): 1237–1244.
- [27] CHIU K Y, WONG M H, CHENG F T, MAN H C. Characterization and corrosion studies of fluoride conversion coating on degradable Mg implants [J]. *Surface and Coatings Technology*, 2007, 202(3): 590–598.
- [28] ZENG Rong-chang, LIU Zhen-guo, ZHANG Fen, LI Shuo-qi, CUI Hong-zhi, HAN En-hou. Corrosion of molybdate intercalated hydrotalcite coating on AZ31 Mg alloy [J]. *Journal of Materials Chemistry A*, 2014, 2(32): 13049–13057.
- [29] ZHANG Fen, LIU Zhen-guo, ZENG Rong-chang, LI Shuo-qi, CUI Hong-zhi, SONG Liang, HAN En-hou. Corrosion resistance of Mg–Al–LDH coating on magnesium alloy AZ31 [J]. *Surface and Coatings Technology*, 2014, 258: 1152–1158.
- [30] MONTEMOR M F, SIMOES A M, CARMEZIM M J. Characterization of rare-earth conversion films formed on the AZ31 magnesium alloy and its relation with corrosion protection [J]. *Applied Surface Science*, 2007, 253(16): 6922–6931.
- [31] LI Ling-jie, LEI Jing-lei, YU Sheng-hai, TIAN Yu-jing, JIANG Qi-quan, PAN Fu-sheng. Formation and characterization of cerium conversion coatings on magnesium alloy [J]. *Journal of Rare Earths*, 2008, 26(3): 383–387.
- [32] RUDD A L, BRESLIN C B, MANSFELD F. The corrosion protection afforded by rare earth conversion coatings applied to magnesium [J]. *Corrosion Science*, 2000, 42(2): 275–288.
- [33] CAI Jing-shun, CAO Fa-he, CHANG Lin-rong, ZHENG Jun-jun, ZHANG Jian-qing, CAO Chu-nan. The preparation and corrosion behaviors of MAO coating on AZ91D with rare earth conversion precursor film [J]. *Applied Surface Science*, 2011, 257(8): 3804–3811.
- [34] SONG Ying-wei, SHAN Da-yong, CHEN Rong-shi, ZHANG Fan, HAN En-hou. Formation mechanism of phosphate conversion film on Mg–8.8 Li alloy [J]. *Corrosion Science*, 2009, 51(1): 62–69.
- [35] ZENG Rong-chang, LAN Zi-dong, CHEN Jun, MO Xian-hua, HAN En-hou. Progress of chemical conversion coatings on magnesium alloys [J]. *The Chinese Journal of Nonferrous Metals*, 2009, 19(3): 397–404. (in Chinese)
- [36] NIU L Y, JIANG Z H, LI G Y, GU C D, LIAN J S. A study and application of zinc phosphate coating on AZ91D magnesium alloy [J]. *Surface and Coatings Technology*, 2006, 200(9): 3021–3026.
- [37] NGUYEN V P, MOON S, CHANG D Y, LEE K H. Effect of microstructure on the zinc phosphate conversion coatings on magnesium alloy AZ91 [J]. *Applied Surface Science*, 2013, 264(1): 70–78.
- [38] NGUYEN V P, LEE K H, CHANG D Y, MOON S. Effects of Zn²⁺ concentration and pH on the zinc phosphate conversion coatings on AZ31 magnesium alloy [J]. *Corrosion Science*, 2013, 74: 314–322.
- [39] NGUYEN V P, LEE K H, CHANG D Y, KIM M, LEE S, MOON S. Zinc phosphate conversion coatings on magnesium alloys: A review [J]. *Metals and Materials International*, 2013, 19(2): 273–281.
- [40] CHEN X B, ZHOU X, ABBOTT T B, EASTON M A, BIRBILIS N. Double-layered manganese phosphate conversion coating on magnesium alloy AZ91D: Insights into coating formation, growth and corrosion resistance [J]. *Surface and Coatings Technology*, 2013, 217(25): 147–155.
- [41] CUI Xue-jun, LIU Chun-hai, YANG Rui-song, FU Qing-shan, LIN Xiu-zhou, GONG Min. Duplex-layered manganese phosphate conversion coating on AZ31 Mg alloy and its initial formation mechanism [J]. *Corrosion Science*, 2013, 76: 474–485.
- [42] LIU Feng, SHAN Da-yong, HAN En-hou, LIU Chang-sheng. Barium phosphate conversion coating on die-cast AZ91D magnesium alloy [J]. *Transactions of Nonferrous Metals Society of China*, 2008, 18(S1): s344–s348.
- [43] TAKAHIRO I, YOSHITAKE M, KATSUYA T. Composite film formed on magnesium alloy AZ31 by chemical conversion from molybdate/phosphate/fluorinate aqueous solution toward corrosion protection [J]. *Surface and Coatings Technology*, 2013, 217(25): 76–83.
- [44] ZHANG Chun-yan, ZENG Rong-chang, CHEN Rong-shi, LIU Cheng-long, GAO Jia-cheng. Preparation of calcium phosphate coatings on Mg–1.0 Ca alloy [J]. *Transactions of Nonferrous Metals Society of China*, 2010, 20(S2): s655–s659.
- [45] HELLER D K, FAHRENHOLTZ W G, O'KEEFE M J. The effect of post-treatment time and temperature on cerium-based conversion coatings on Al 2024-T3 [J]. *Corrosion Science*, 2010, 52(2): 360–368.
- [46] WU G S, IBRAHIM J M, CHU P K. Surface design of biodegradable magnesium alloys—A review [J]. *Surface and Coatings Technology*, 2013, 233(25): 2–12.
- [47] LI Qing, XU Shu-qiang, HU Jun-ying, ZHANG Shi-yan, ZHONG Xian-kang, YANG Xiao-kui. The effects to the structure and electrochemical behavior of zinc phosphate conversion coatings with ethanolamine on magnesium alloy AZ91D [J]. *Electrochimica Acta*, 2010, 55(3): 887–894.
- [48] ZENG Rong-chang, LAN Zi-dong. Influence of bath temperature of conversion treatment process on corrosion resistance of zinc calcium

- phosphate conversion film on AZ31 magnesium alloy [J]. The Chinese Journal of Nonferrous Metals, 2010, 20(8): 1461–1466.
- [49] ZENG Rong-chang, LAN Zi-dong, KONG Ling-hong, HUANG Yuan-ding, CUI Hong-zhi. Characterization of calcium-modified zinc phosphate conversion coatings and their influences on corrosion resistance of AZ31 alloy [J]. Surface and Coatings Technology, 2011, 205(11): 3347–3355.
- [50] ZENG Rong-chang, ZHANG Fen, LAN Zi-dong, CUI Hong-zhi, HAN En-hou. Corrosion resistance of calcium-modified zinc phosphate conversion coatings on magnesium–aluminium alloys [J]. Corrosion Science, 2014, 88: 452–459.
- [51] HUSSEIN A M, GARDNER P J, MCARA I W. The standard enthalpies of formation of some zinc orthophosphate polymorphs [J]. Thermochemica Acta, 1992, 196(1): 117–123.
- [52] ZENG Rong-chang, SUN Xin-xin, SONG Ying-wei, ZHANG Fen, LI Shuo-qi, CUI Hong-zhi, HAN En-hou. Influence of solution temperature on corrosion resistance of Zn–Ca phosphate conversion coating on biomedical Mg–Li–Ca alloys [J]. Transactions of Nonferrous Metals Society of China, 2013, 23(11): 3293–3299.
- [53] XU Luo-min, WANG Xi, LI Lei, KE Zuo. Densification process of cerium-based conversion coatings on AZ31 magnesium alloy [J]. The Chinese Journal of Nonferrous Metals, 2013, 23(11): 3135–3140. (in Chinese)
- [54] ZHANG Mi-lin. Cerium chemical conversion coating on a novel Mg–Li alloy [J]. Journal of Wuhan University of Technology: Materials Science Edition, 2010, 25(1): 112–117.
- [55] ZENG R C, ZHANG J, HUANG W J, DIETZEL W, KAINER K U, BLAWERT C, KE W. Review of studies on corrosion of magnesium alloys [J]. Transactions of Nonferrous Metals Society of China, 2006, 16(S1): s763–s771.

AZ31 镁合金表面铈掺杂 锌钙磷酸盐化学转化膜的腐蚀性能

曾荣昌^{1,2}, 胡艳^{1,2}, 张芬^{1,2}, 黄原定⁴, 王振林³, 李硕琦^{1,2}, 韩恩厚⁵

1. 山东科技大学 材料科学与工程学院, 青岛 266590;

2. 山东科技大学 山东省矿山灾害预防控制重点实验室—省部共建国家重点实验室培育基地, 青岛 266590;

3. 重庆理工大学 材料科学与工程学院, 重庆 400054;

4. MagIC–Magnesium Innovation Center, Helmholtz-Zentrum Geesthacht,

Zentrum für Material-und Küstenforschung GmbH, Geesthacht D-21502, Germany;

5. 中国科学院 金属研究所 国家金属腐蚀控制工程技术研究中心, 沈阳 110016

摘要: 在 AZ31 镁合金表面制备锌钙磷酸盐(Zn–Ca–P)涂层和铈掺杂锌钙磷酸盐(Zn–Ca–Ce–P)涂层。采用 X 射线能谱(EDS)、光电子能谱(XPS)、X 射线衍射(XRD)、电子探针(EPMA)和扫描电镜(SEM)以及析氢实验和电化学测试技术研究涂层的化学成分、形貌和腐蚀性能。结果表明: 两种膜层主要是磷酸盐($Zn_3(PO_4)_2 \cdot 4H_2O$)、 $Mg_3(PO_4)_2$ 、 $Ca_3(PO_4)_2$ 晶体簇和少量的 MgF_2 和 CaF_2 非晶颗粒组成。 $CePO_4$ 的形成使 Zn–Ca–Ce–P 膜层更加致密, 并具有更好的耐蚀性。两种涂层只能在浸泡前期为 AZ31 镁基体提供保护作用, 随着浸泡时间延长, 涂层与基体界面之间电偶腐蚀的发生加快了腐蚀速率。 Ce 的添加促进了 Ca 的均匀分布和磷化膜的形成。因此, Zn–Ca–Ce–P 涂层具有作为镁合金底涂层的应用前景。

关键词: AZ31 镁合金; 铈; 锌钙磷酸盐; 化学转化膜; 腐蚀性能

(Edited by Mu-lan QIN)